Periodic plasma escape from the mass-loaded Kronian magnetosphere

B. Zieger,[1,2,3] K. C. Hansen,[1] T. I. Gombosi,[1] and D. L. De Zeeuw[1]

Received 1 October 2009; revised 29 December 2009; accepted 30 March 2010; published 10 August 2010.

[1] We use a single-fluid global MHD model to study the solar wind control of large-scale mass loading and plasma release phenomena in the Kronian magnetosphere. We show that, at high solar wind dynamic pressure, the loss of plasma in the magnetotail is continuous. At medium dynamic pressure, plasmoids are pinched off periodically along an X-line in the postmidnight sector through a cascade of helical reconnection. Plasmoids have a magnetic topology of a helical flux rope with its ends anchoring in the polar regions of Saturn. With decreasing dynamic pressure, the repetition period of plasmoids gradually increases. A higher mass-loading rate or a higher axial tilt of Saturn makes the repetition period longer. At low dynamic pressure, the release of plasmoids becomes quasi-periodic or chaotic. The pressure control of the repetition period is very similar to the behavior of a dripping faucet. The mass and volume of the closed magnetosphere are smaller at lower dynamic pressures because of a relatively longer X-line. In our simulations, large-scale plasmoids are responsible for less than 8% of the total mass loss, and the rest of the plasma is lost via cross-field diffusion or other small-scale mechanisms.

Citation: Zieger, B., K. C. Hansen, T. I. Gombosi, and D. L. De Zeeuw (2010), Periodic plasma escape from the mass-loaded Kronian magnetosphere, *J. Geophys. Res.*, *115*, A08208, doi:10.1029/2009JA014951.

1. Introduction

[2] The magnetospheres of the giant planets, like Jupiter and Saturn, are fundamentally different from the terrestrial magnetosphere. Besides the relatively fast rotation rate of these planets, there are significant mass-loading sources in these magnetospheres, which were identified as Io in the case of Jupiter [*Broadfoot et al.*, 1979; *Shemansky*, 1980; *Pontius and Hill*, 1982; *Brown*, 1994; *Bagenal*, 1994, 1997; *Kivelson et al.*, 1996; *Russell et al.*, 2001; *Wang et al.*, 2001; *Saur et al.*, 2003] and Enceladus, as the dominant one, in the case of Saturn [*Shemansky et al.*, 1993; *Richardson*, 1998; *Jurac et al.*, 2002; *Dougherty et al.*, 2006; *Porco et al.*, 2006; *Leisner et al.*, 2006; *Pontius and Hill*, 2006; *Khurana et al.*, 2007; *Tokar et al.*, 2008; *Cowee et al.*, 2009]. The neutral cloud produced by these satellites is partly ionized through charge exchange, photoionization, or electron impact ionization, resulting in a more or less azimuthally symmetric plasma source. The internally generated magnetospheric plasma forms a bowl-shaped plasma sheet around Saturn [*Arridge et al.*, 2008] and tends to inflate the magnetosphere by stretching the magnetic flux tubes at low latitudes, especially on the night side. Eventually, the extra mass added by the magnetospheric source needs to leave the magnetosphere.

[3] A general pattern of plasma convection in the Jovian magnetosphere was qualitatively described by *Vasyliũnas* [1983] and *Kivelson and Southwood* [2005] and may be applicable to the rotationally driven Kronian magnetosphere as well. The Vasyliũnas model predicts an X-line in the midnight-dawn sector, where the overstretched closed magnetic field lines reconnect, releasing a plasmoid in the magnetotail. Such large-scale plasmoids with a repetition period of 1–3 days were inferred from in situ Galileo measurements in Jupiter's near tail [*Russell et al.*, 2000; *Woch et al.*, 2002; *Bagenal*, 2007] and were confirmed more recently with observations by the New Horizons spacecraft far down the Jovian magnetotail [*Krupp*, 2007; *McComas et al.*, 2007]. Several plasmoid events were reported in Saturn's magnetotail in the course of the Cassini mission [*Jackman et al.*, 2007, 2008; *Hill et al.*, 2008], although these single-orbit observations did not allow for the determination of any repetition period.

[4] Here we use an MHD model of the mass-loaded Kronian magnetosphere, as described in section 2, to simulate large-scale plasma loss phenomena, including periodic plasmoids, under a wide range of upstream solar wind conditions. The simulation results are presented and discussed in sections 3 and 4, and our general conclusions on the solar wind dynamic pressure control of plasma loss in the Kronian magnetosphere are drawn in section 5.

2. Numerical Model

[5] Our single-fluid 3-D MHD model of the mass-loaded Kronian magnetosphere is implemented within the Space Weather Modeling Framework [*Tóth et al.*, 2005] through

[1]Department of Atmospheric, Oceanic and Space Sciences, University of Michigan, Ann Arbor, Michigan, USA.
[2]Also at Geodetic and Geophysical Research Institute, Hungarian Academy of Sciences, Sopron, Hungary.
[3]Now at Space Research Institute, Austrian Academy of Sciences, Graz, Austria.

0148-0227/10/2009JA014951

the coupling of global magnetosphere (BATS-R-US) [*Powell et al.*, 1999] and ionosphere electrodynamics components. The latter is a height-integrated electric potential solver, which uses field-aligned currents to calculate particle precipitation and conductance [*Ridley et al.*, 2004]. In the simulations presented here, we apply the simplest ionosphere model with a uniform Pedersen conductance. The global MHD model was adapted to Saturn by including mass-loading source terms in the MHD equations (for details see *Hansen et al.* [2000]) and was further improved by adjusting the spatial distribution of magnetospheric plasma sources as well as the mass-loading rates to more recent observations [*Hansen et al.*, 2005]. The major plasma source of water group ions W^+ (H_2O^+, OH^+, O^+) from Enceladus and the rings is taken into account as an axisymmetric disc-like source centered at 5.35 Saturn radii (R_S), while a secondary plasma source of nitrogen ions N^+ from Titan is modeled with an axisymmetric torus at Titan's orbit. The functional forms of the assumed neutral density distributions, as described by *Hansen et al.* [2005], were based on the observational and modeling results of *Richardson et al.* [1998] and *Ip* [1992], respectively. Although the Cassini mission has improved our knowledge of the spatial distribution of the neutral cloud, the global MHD simulations of Saturn's magnetosphere are expected to be more sensitive to the total mass-loading rate than to the distribution of the inner magnetospheric plasma sources.

[6] In our model, we assume a nominal mass-loading rate of 3×10^{27} s^{-1} for W^+ and 5×10^{25} s^{-1} for N^+. The total mass-loading rate of plasma amounts to 84.5 kg/s assuming an average mass of 16.6 amu for W^+ and 14 amu for N^+. As reference, the estimates of total H_2O source rates or neutral cloud erosion rates range from 1.4×10^{27} s^{-1} [*Richardson et al.*, 1998], to $>4 \times 10^{27}$ s^{-1} [*Pontius and Hill*, 2006], to 2.26×10^{26} s^{-1} [*Leisner et al.*, 2006], which was corrected by the authors to 2×10^{27} s^{-1} according to *Cowee et al.* [2009], up to 6×10^{27} to 1.4×10^{28} s^{-1} [*Cowee et al.*, 2009]. Furthermore, *Burger et al.* [2007] suggested an H_2O source rate as high as 10^{28} s^{-1} originating from the southern Enceladus plume only. To obtain an idea of the ion mass-loading rate, we must understand the ionization processes at Saturn. *Richardson and Jurac* [2004] found that the majority of neutrals escape the system without being ionized and that only 30% of the neutrals are ionized in the magnetosphere and contribute to the ion mass loading. The plasma mass-loading rate is a free parameter in our MHD model, which can be used to tune the simulation results to the observations. The current value is well within the various estimated rates and was determined by comparison with Cassini measurements of bow shock and magnetopause crossings [*Hansen et al.*, 2005]. Because we aim at discussing the large-scale phenomenological behavior of the Kronian magnetosphere under different solar wind dynamic pressure conditions, fine-tuning the mass-loading rate is not a crucial issue here.

[7] The dimensions of the simulation domain are −576 to 96 R_S in the X direction, and −192 to 192 R_S in the Y and Z directions, where X, Y, and Z are the Kronocentric solar magnetospheric coordinates: X points toward the Sun, Y is perpendicular to the dipole axis, which is practically the same as the rotation axis in the case of Saturn and points toward dusk, and Z is chosen so that the dipole axis or rotation axis lies in the $X - Z$ plane. In most of the simulations discussed in this study, the axial tilt of Saturn, that is, the angle between X and the rotation axis, was chosen to be −8.91°, one third of the maximum absolute tilt of 26.73° at Kronian solstices. Owing to an automatic mesh refinement algorithm the grid resolution is highest in the regions of interest: the inner equatorial plane, the bow shock, the magnetopause, and the cross-tail current sheet. The resolution around the mass-loading region of the icy satellites is 3/16 R_S, at Titan it is 3/8 R_S, while the largest computational cells (6 R_S) are located far downtail in the magnetotail lobes. The inner boundary of the computational domain is at a radial distance of 3 R_S.

3. Simulation Results

3.1. Upstream Solar Wind at Saturn

[8] Our goal is to explore the solar wind dynamic pressure control of the Kronian magnetosphere; therefore, it is essential to know the typical upstream solar wind conditions at Saturn as well as the expected range of the solar wind dynamic pressure. Because in situ upstream solar wind observations are rather scarce, we used the Michigan Solar Wind Model (http://mswim.engin.umich.edu/) to propagate the solar wind from 1 AU to Saturn. This one-dimensional MHD model of the solar wind was described and sufficiently validated against Pioneer, Voyager, and Cassini observations by *Zieger and Hansen* [2008]. On the basis of 14 years of propagated solar wind data from 1995 to 2008, covering more than a solar cycle, we derived distribution functions and the median values of all the MHD variables at Saturn, which then were used as upstream boundary conditions in the 3-D MHD simulations of Saturn's magnetosphere. For the interplanetary magnetic field (IMF), we assumed an ideal Parker spiral with the typical values B_x = −0.018 nT and B_y = 0.17 nT, corresponding to the away IMF sector. The value of B_z was kept zero in all but two simulations to suppress the Dungey cycle of field line reconnection as much as possible. The upstream plasma temperature was set to 2×10^4 K in all cases. We assumed a purely radial solar wind flow at a speed of 400 km/s and regulated the solar wind dynamic pressure (p_{sw}) by varying the density.

[9] The probability density function of ln p_{sw} is shown in Figure 1. The distribution of p_{sw} is very close to a lognormal distribution. We do not find a bimodal distribution of solar wind dynamic pressures as found by previous authors at Jupiter [*Joy et al.*, 2002] or which might serve as a reason for an apparent bimodal magnetopause location at Saturn [*Achilleos et al.*, 2008]. The median p_{sw} is 12.6 pPa, whereas the interquartile range, containing 50% of the data, ranges from 5.2 to 28 pPa. The distribution extends as low as 0.8 pPa (1st percentile) and as high as 155.8 pPa (99th percentile). In this paper, we refer to dynamic pressures below the lower quartile as low ($p_{sw} < 5.2$ pPa), within the interquartile range as medium (5.2 pPa $< p_{sw} <$ 28 pPa), and above the upper quartile as high ($p_{sw} > 28$ pPa).

3.2. Magnetic Topology of Plasmoids

[10] We completed a series of 3-D MHD simulations of the Kronian magnetosphere covering the meaningful range of p_{sw}, from 2 through 150 pPa, maintaining steady

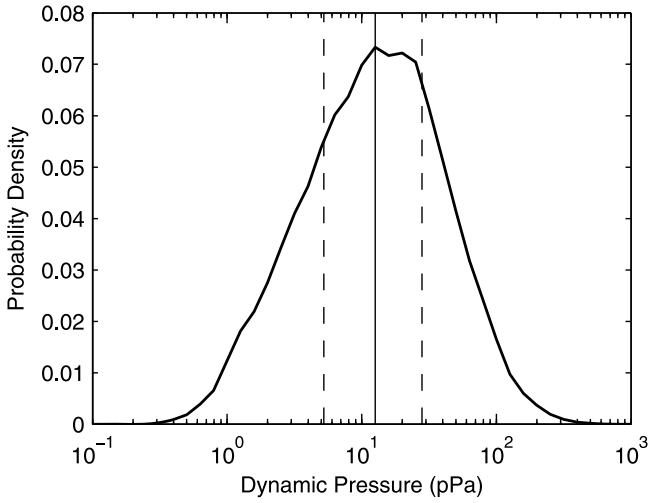

Figure 1. Probability density function of solar wind dynamic pressure at Saturn for the period 1995–2008. The median of the distribution is marked with a vertical solid line, while the lower and upper quartiles are indicated with dashed lines.

upstream solar wind boundary conditions in each case. Each run was continued up to 400 simulation hours. The simulations converge typically after 150–180 h, when the magnetosphere has become completely filled up by the magnetospheric plasma sources defined in section 2. Interestingly enough, the MHD solution results in a steady state Kronian magnetosphere only for high p_{sw} (>28 pPa). For medium p_{sw}, periodic oscillations are observed in the total mass of the simulation box, in the volume and mass of the closed magnetosphere, in the total field-aligned currents, in the ionospheric transpolar potential, as well as in the bow shock and magnetopause locations. These perturbations gradually become quasi-periodic as p_{sw} drops below the median (12.6 pPa). The perturbation of the closed magnetospheric mass indicates that a part of the magnetospheric plasma leaves the system in a quantized manner rather than continuously.

[11] Indeed, the simulations show periodic or quasi-periodic release of large plasmoids in the postmidnight sector of the Kronian near tail for medium and low p_{sw}. The structure of the closed Kronian magnetosphere and the magnetic topology of a plasmoid are illustrated in Figure 2. In the premidnight sector, the last closed field lines extend over 300 R_S downtail, whereas in the postmidnight sector an X-line is formed in the near tail. The X-line starts premidnight at a radial distance of about 40–50 R_S and bends upstream so that it is closer to Saturn on the dawn side. When the last closed field lines are stretched sufficiently beyond the prospective X-line owing to the magnetospheric mass loading and the fast rotation of the planet, a cascade of helical reconnection is triggered along the X-line, where a closed overstretched field line reconnects in fact not to itself, which would produce a magnetic O, but to an adjacent closed field line producing a magnetic helix. The resulting helical flux rope remains magnetically connected to the planet at both ends. Thus, the Vasyliũnas-type plasmoids are confined in long helical flux ropes that are mapped to a small foot point

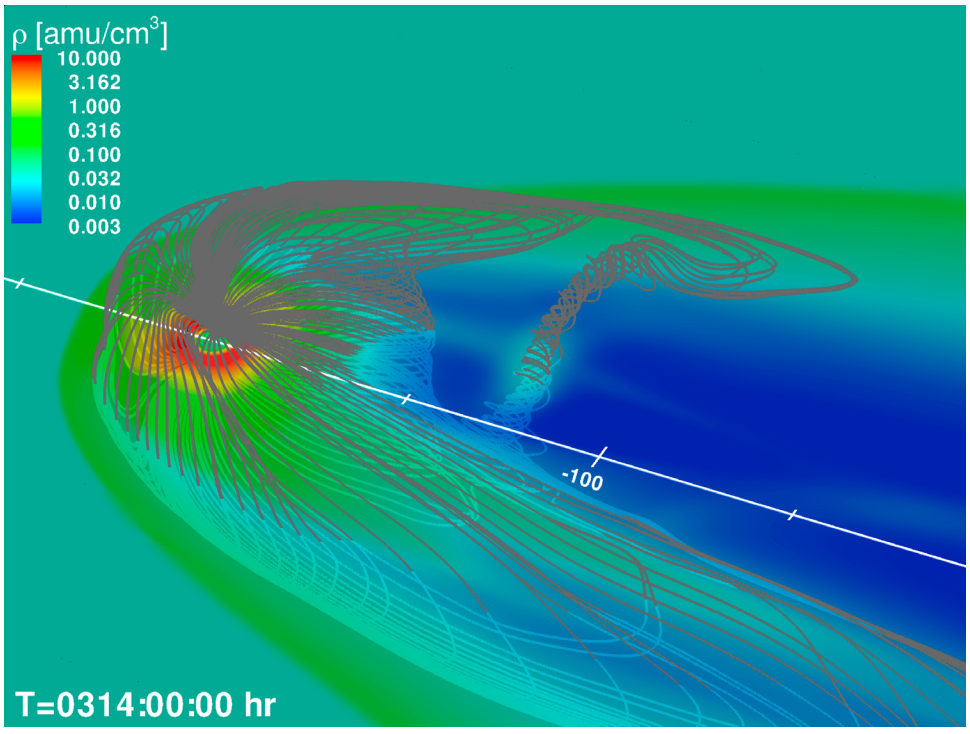

Figure 2. Helical flux rope-like plasmoid having pinched off along the Vasyliũnas X-line in a simulation with p_{sw} = 8.6 pPa and an axial tilt of −8.91°. The last closed field lines are plotted in gray and white above and below the z = 0 plane, respectively.

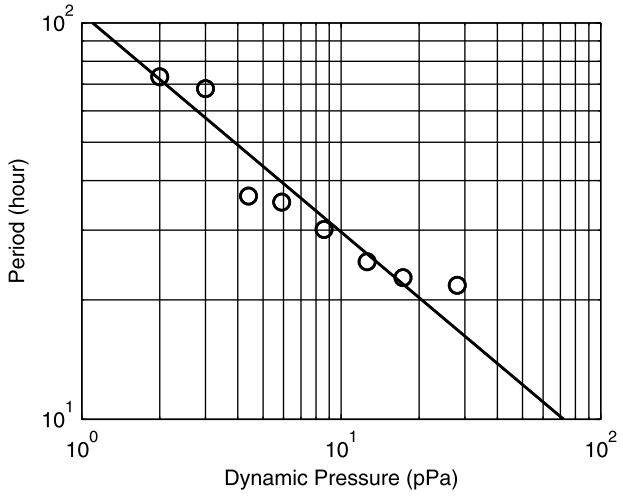

Figure 3. Repetition period of plasmoid release as a function of solar wind dynamic pressure for an axial tilt of −8.91°. The best-fitting power law function is plotted as a solid line.

in each polar region of Saturn (see Figure 2). It is likely that the cascade-like tail reconnection and the related plasmoid release are associated with some very small scale periodic auroral phenomenon. Interestingly enough, the cascade of helical reconnection can start either at midnight, propagating toward dawn, or at dawn, propagating toward midnight, so plasmoids can be zipped off both ways along the X-line depending on local plasma instabilities. Once released, plasmoids rapidly expand while drifting down in the void of the dawnside tail. The length of the Vasyliũnas X-line, and consequently the size or mass of a plasmoid, is determined by p_{sw}, as discussed in section 3.4.

3.3. Repetition Period of Plasmoids

[12] The repetition period of plasmoids can be derived from the periodic or quasiperiodic perturbation of the mass of the closed magnetosphere. The closed magnetospheric mass reaches a local maximum just before a plasmoid is released and drops to a local minimum right after the plasmoid has completely pinched off. In the simulations, the closed magnetospheric mass is calculated every 5 min by integrating the plasma density along closed magnetic flux ropes. Here we define the repetition frequency as the dominant peak in the Fourier spectrum of the closed magnetospheric mass perturbation within the time interval between 180 and 400 simulation hours. Very similar repetition periods are obtained when analyzing other time-varying simulation parameters. The repetition period of plasmoids gradually increases with decreasing p_{sw} from ~20 to ~70 h in the medium- and low-p_{sw} regime as shown in Figure 3. The best-fitting power law function $T = 105.6\ p_{sw}^{-0.551}$ (solid line in Figure 3) provides the relation between the repetition period T and p_{sw} for an axial tilt of −8.91°, where T and p_{sw} are given in units of hours and pPa, respectively. In the high-p_{sw} regime (>28 pPa), we could not identify any periodic perturbation in the total mass, which means that the magnetospheric plasma is lost more or less continuously. The Fourier spectrum of the closed magnetospheric mass perturbation becomes broader and broader for the lower tail of the p_{sw} distribution, which means that the release of plasmoids is becoming more and more chaotic.

[13] The results shown in Figure 3 are valid for a closed magnetospheric configuration with no or negligible Dungey-type field-line reconnection, which corresponds to negative or zero IMF B_z, because the dipole moment of Saturn points northward, unlike the dipole moment of Earth, which points southward. To test the effect of the Dungey cycle on the frequency of plasmoid release, we ran two additional simulations at 2 pPa with negative and positive B_z (±0.043 nT), although in reality it is very unlikely that B_z would remain either positive or negative for 400 h. We obtained a repetition period of 64 h for negative B_z, which is comparable to that of 73.1 h in the case of zero B_z. However, the simulation with positive B_z, or open magnetospheric configuration, yielded a significantly lower period of 48.8 h.

[14] The repetition period T also depends on the axial tilt or Saturn season. At a medium p_{sw} of 17.3 pPa, T increases with the tilt angle, as 22.5, 24.3, and 29.2 h for 1/3, 2/3, and 3/3 of the maximum tilt of 26.73° at solstices, respectively. Oddly enough, no large-scale plasmoids are produced in a simulation with zero tilt, corresponding to Kronian equinox, at least at medium p_{sw} under steady upstream solar wind conditions. As a possible explanation, we suggest that the cascade of helical reconnection described in section 3.2 may not be triggered in a perfectly north–south symmetric magnetic field configuration.

[15] We also examined the influence of the mass-loading rate on the repetition period of plasmoids. If the plasma mass-loading rate is raised from the nominal value of 3×10^{27} ions/s to 10^{28} ions/s at a medium p_{sw} of 17.3 pPa, T will increase from 22.6 to 64 h. On the other hand, a lower mass-loading rate of 10^{27} ions/s would result in a repetition period of 9.8 h at the same p_{sw}; however, the amplitude of the periodic perturbation would become much smaller.

3.4. Mass and Volume of the Closed Magnetosphere

[16] On the basis of spacecraft measurements in a real magnetosphere, it is very hard to estimate the actual volume of the magnetosphere and how much plasma is confined in the closed part of the magnetosphere. Similarly, based on a single encounter of a spacecraft with a plasmoid, one can tell hardly anything about the actual size and mass of the plasmoid. In an MHD simulation, these quantities can be directly calculated. As already mentioned, the mass of the closed magnetosphere is calculated in our simulations every 5 min by means of a ray-tracing algorithm. The total volume of the closed magnetosphere is calculated and saved every 5 min in a similar manner. In this section we investigate how these quantities respond to changes in p_{sw}.

[17] The mass and volume of the closed magnetosphere as a function of p_{sw} are plotted in Figures 4 and 5, respectively. Surprisingly, both of these quantities tend to decrease with decreasing p_{sw} in the medium- and low-p_{sw} regime, although the standoff distance of the magnetosphere increases following a power law scaling relation due to the pressure balance at the magnetopause. In the high-p_{sw} regime (>28 pPa), however, where no plasmoids are observed, the volume of the closed magnetosphere increases with decreasing p_{sw} as expected (see Figure 5). Thus, the unusual

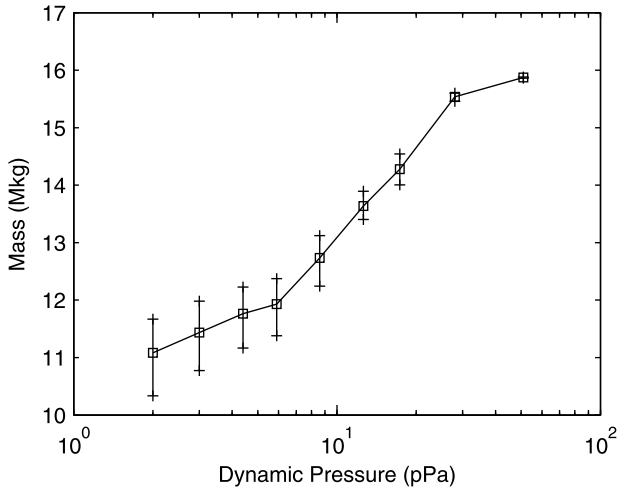

Figure 4. Mass of the closed magnetosphere for an axial tilt of −8.91°. The error bars indicate the range of mass in each simulation.

behavior of the closed magnetospheric mass and volume must be related to plasmoid release.

[18] If the Kronian magnetosphere were self-similar (e.g., similar to the one shown in Figure 2), all of its dimensions would scale with p_{sw} like the standoff distance, and hence the volume of the closed magnetosphere would increase with decreasing p_{sw}, which is clearly not the case in our simulations. We found that it is the length of the reconnection line that scales differently. The relative length of the X-line with respect to the dawn-dusk diameter of the magnetotail increases with decreasing p_{sw}. A relatively longer X-line removes a larger percentage of the closed magnetotail in the postmidnight sector, which results in the decreased volume and mass of the closed magnetosphere.

[19] The range of the closed magnetospheric mass is indicated with error bars in Figure 4, which gives a rough estimate of the mass of individual plasmoids. The length of the error bars or the mass of plasmoids seems to increase with decreasing p_{sw}. This can be explained with a longer X-line that produces a longer helical flux rope and thus a more massive plasmoid.

[20] Comparing the figures of the closed magnetospheric mass and the closed magnetospheric volume (Figures 4 and 5), one can find that the relative ranges of the volume (error bars in Figure 5) are much larger than the relative ranges of the mass (error bars in Figure 4). In other words, the volume of the closed magnetosphere is much more variable than the mass of the closed magnetosphere. This implies that a major part of the magnetospheric volume perturbation is caused by compression and expansion and only a smaller part is caused by volume loss via plasmoid release. The periodic release of plasmoids undoubtedly results in a periodic pressure perturbation in the magnetosphere, which propagates in the form of sound waves. The magnetosphere tries to counteract this perturbation by periodic expansion and compression. This kind of periodic "breathing" of the closed magnetosphere leads to periodic perturbations of the magnetopause and bow shock locations in the simulations, which can be the reason for the dual distributions of bow shock and magnetopause locations observed in the Jovian and Kronian magnetospheres [*Joy et al.*, 2002; *Achilleos et al.*, 2008].

[21] The average masses of large-scale plasmoids were calculated for each simulation using the differences between local maxima and the subsequent local minima in the mass of the closed magnetosphere within the simulation interval between 300 and 400 h. The results are plotted in Figure 6 with open circles. The average mass of plasmoids steadily increases with decreasing p_{sw} from 0.1 Mkg at 28 pPa up to 1.35 Mkg at the lowest p_{sw} of 2 pPa. Because the mass of the closed magnetosphere decreases with decreasing p_{sw} (see Figure 4), a greater and greater fraction of the closed magnetospheric mass can be lost with a single event of plasmoid release. At 2 pPa, this fraction becomes as high as 12%.

[22] Knowing the average mass of plasmoids and the repetition period of plasmoids (see Figure 3), we can calculate the mass loss rate via large-scale plasmoids in kg/s that is plotted in Figure 6, too (asterisks). The efficiency of mass loss via large-scale plasmoids seems to peak at 8.6 pPa, where about 6.5 kg plasma is lost every second on average. This is less than 8% of the total mass-loading rate of 84.5 kg/s used in the simulations. Thus, a significant part of the magnetospheric plasma must be lost continuously, most probably through cross-field diffusion. In the case of our simulations in the high-p_{sw} regime at 51 and 150 pPa with no apparent large-scale plasmoids, all the internally loaded plasma is lost continuously. At low p_{sw}, the mass-loss rate via large-scale plasmoids tends to decline as alternative forms of plasma loss come into play (e.g., trains of bigger and smaller plasmoids, plasma shedding in the premidnight sector of the closed magnetotail, or episodic dayside plasma injections from the plasma disc into the magnetosheath).

[23] One may notice in Figure 6 that the efficiency of mass loss via large-scale plasmoids seems to peak at dynamic pressures where the corresponding repetition period is close to multiples of the rotation period (compare with Figure 3). This may hint to certain resonance states of the magneto-

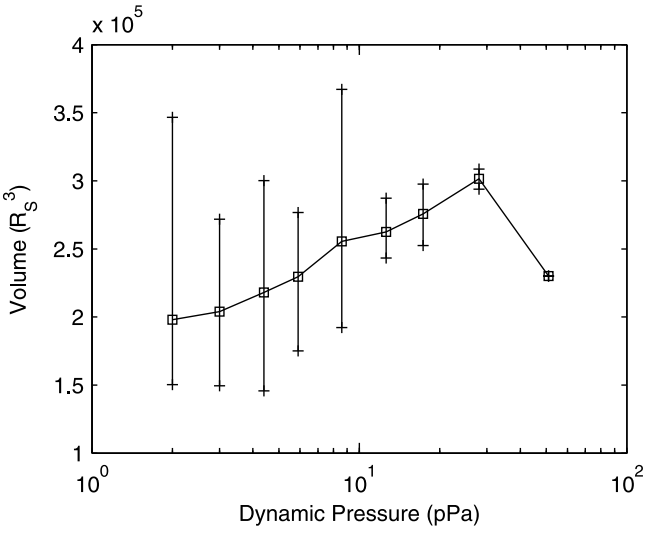

Figure 5. Volume of the closed magnetosphere for an axial tilt of −8.91°. The error bars indicate the range of volume in each simulation.

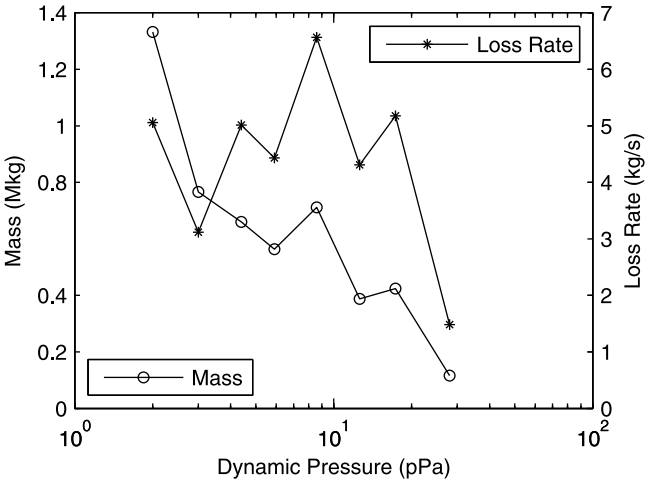

Figure 6. Mass loss via plasmoid release for an axial tilt of −8.91°. The left-hand scale shows the average mass of plasmoids, while the right-hand scale shows the mass loss rate via plasmoids.

sphere, but such a hypothesis could be tested only with a large number of additional simulations.

4. Discussion

[24] Our simulations demonstrate that the Vasyliũnas cycle [*Vasyliũnas*, 1983] and the related release of large-scale quasi-periodic plasmoids are important elements of plasma loss not only in the Jovian but also in the Kronian magnetosphere, especially at medium and low solar wind dynamic pressure. Theoretical considerations seem to confirm our modeling results. In a recent paper, *Vasyliũnas* [2008] pointed out that the mass-loading rates of different planetary magnetospheres should be compared in a normalized unit, where the planetary dipole moment, the planetary rotation rate, and the radial distance of the mass-loading source are used as scaling parameters. Although the absolute mass-loading rate of Io in the Jovian magnetosphere is at least an order of magnitude higher than the absolute mass-loading rate of Enceladus in the Kronian magnetosphere, the scaled mass-loading rate of Saturn is still about 6 times higher than that of Jupiter [*Vasyliũnas*, 2008].

[25] The Vasyliũnas model suggests an X-line in the midnight-dawn sector of the tail where the overstretched closed magnetospheric field lines reconnect to themselves, releasing a plasmoid down the tail. The recently emptied flux tubes rapidly move toward Saturn until they are gradually refilled with magnetospheric plasma and stretched in the tail again. Our simulations confirm this mechanism of plasma loss, but the O-type reconnection described in the Vasyliũnas model transforms into a cascade of helical reconnection in a more general 3-D geometry. The reconnection propagates along the X-line either from dawn toward midnight or from premidnight toward dawn until a large-scale plasmoid is completely pinched off.

[26] Plasmoids are confined in a long helical flux rope with its ends magnetically mapping into the polar regions of Saturn (see Figure 2), which might result in some kind of small-scale periodic auroral activity. Having pinched off, plasmoids start to expand while drifting downstream in the void of the tail lobes, and they finally connect to the dawnside magnetopause, injecting magnetospheric plasma into the magnetosheath. The magnetic topology of Kronian plasmoids is very similar to the arched topology of coronal streamer blobs, where the legs of the helical magnetic flux ropes are anchored in the Sun [*Wang et al.*, 2000; *Wang and Sheeley*, 2006; *Sheeley and Wang*, 2007; *Sheeley et al.*, 2009]. The helical reconnection process and the detachment mechanism of plasma blobs seem to be very similar in the solar corona and in the dawnside magnetotail of Saturn.

[27] Keeping the Vasyliũnas model in mind, it is straightforward to explain the solar wind control of the size and frequency of plasmoids presented in section 3. As p_{sw} decreases, the scale size of the magnetosphere increases, and therefore more time and more plasma is needed to fill up a recently emptied flux tube with magnetospheric plasma. A longer X-line also contributes to the increase of plasmoids in size and mass.

[28] If we turn on the Dungey cycle with a positive B_z, the scale size of the magnetosphere decreases because of the dayside field-line reconnection or the "erosion" of closed magnetic field lines. Consequently, the frequency of plasmoid release is expected to increase. For a negative B_z, on the other hand, the size of the magnetosphere does not change significantly, because the magnetosphere remains more or less closed. In this case, the frequency or the repetition period of plasmoid release is not expected to change significantly. Our two additional simulations with positive and negative B_z at 2 pPa support this idea.

[29] The typical repetition period of Kronian plasmoids at medium and low p_{sw} was found to fall in the range between 20 and 70 h in our simulations. We demonstrated that the repetition period can change significantly with the axial tilt of Saturn. Interestingly enough, our model predicts no Vasyliũnas-type plasmoids for the Saturn equinox, probably because of geometric reasons that are not favorable for the helical tail reconnection process. The plasma mass-loading rate also has a significant influence on the repetition period and size of plasmoids. Because there is still a significant uncertainty in the actual plasma mass-loading rate in the Kronian magnetosphere, this parameter can be used to tune the MHD simulation to future observations of periodic plasmoid events.

[30] Our simulations suggest that the closed Kronian magnetosphere is not self-similar in the medium- and low-p_{sw} regime, which means that not all dimensions scale the same way with p_{sw} as the standoff distance. We found that it is the length of the Vasyliũnas X-line that scales differently, getting relatively longer at lower p_{sw}. For this reason, the mass and volume of the closed magnetosphere, surprisingly enough, decreases with decreasing p_{sw}.

[31] Because the mass of plasmoids is proportional to the length of the X-line, the fraction of the closed magnetospheric mass that is released with a single plasmoid is larger at lower p_{sw}, becoming as high as 12% at 2 pPa. Such a dramatic plasmoid event must have tremendous influence on the global magnetospheric configuration and plasma convection pattern, which can significantly distort the equilibrium shape of the magnetopause or bow shock, resulting in huge fluctuations in the magnetopause and bow shock

locations. The largest plasmoids can be as massive as 1.3 Mkg at low p_{sw}, which is comparable to the mass of the whole magnetodisc between 18 and 45 R_S (~10^6 kg) estimated by *Arridge et al.* [2007] on the basis of Cassini observations.

[32] We find that the perturbations in the closed magnetospheric volume are much larger than what is expected from the initial volume of plasmoids. We conclude that this phenomenon is due to global compressional oscillations of the closed magnetosphere, which try to counteract the periodic pressure perturbations associated with the release of plasmoids. The broad distribution of observed Cassini magnetopause crossings [*Achilleos et al.*, 2008] is most probably caused by such global compressional oscillations.

[33] The mass loss rate via regular Vasyliũnas-type plasmoids seems to be most effective at a p_{sw} of 8–9 pPa, but even under such favorable upstream conditions it is not more than 6.5 kg/s. This is less then 8% of the total plasma mass-loading rate of 84.5 kg/s in our simulations. Consequently, a major part of the magnetospheric plasma must be lost continuously through cross-field diffusion or other kinds of small-scale plasma loss mechanisms. *Bagenal* [2007] came to a similar conclusion when estimating the fraction of plasma loss via plasmoids in the Jovian magnetosphere. Assuming a plasmoid repetition period of 1 day, the mass loss rate via plasmoids in the Jovian system amounts to only 1% of the canonical plasma production rate.

5. Conclusions

[34] Summarizing the solar wind dynamic pressure control of plasma loss over the full range of p_{sw} from 2 to 150 pPa, we conclude that the Kronian magnetosphere behaves like a dripping faucet. At high p_{sw}, the loss of plasma in the magnetotail is continuous and the magnetosphere is close to steady state. At medium p_{sw}, the loss of plasma becomes quantized, in a way that large-scale plasmoids are formed and pinched off periodically or quasi-periodically in accordance with the Vasyliũnas cycle. At low p_{sw}, however, internal instabilities lead to nondeterministic plasma dynamics, where the magnetospheric plasma is released chaotically in trains of plasmoids of different size. In fact, p_{sw} controls the scale size of the magnetosphere and the length of the Vasyliũnas X-line in a closed magnetospheric configuration. Thus, it is the variable cross section of the "faucet" that regulates the outflow, because the internal mass-loading rate is constant in the simulations.

[35] Our model predicts a plasmoid repetition period of 20–70 h in the medium- and low-p_{sw} regime, at least for a total plasma mass-loading rate of 84.5 kg/s. An enhanced Dungey cycle would make this typical repetition period shorter, whereas a larger axial tilt would make it longer. On the basis of our simulation results, repetitive plasmoids are expected beyond 40–50 R_S down the tail in the postmidnight sector during long periods of relatively quiet solar wind conditions with low dynamic pressure around Kronian solstices. The model does not produce plasmoids at Kronian equinoxes. Because plasmoids are curved flux ropes that are pinched off along the X-line, they intersect the equatorial plane only in a limited local time sector, especially at closer radial distances. The best chance of observing repetitive plasmoids is farther down the tail, because plasmoids rapidly expand while convecting downstream. The reason why Cassini has observed only five to six plasmoids so far must be attributed to its orbit in the first place besides the aforementioned seasonal and solar wind effects.

[36] In general, we conclude that internal instabilities and plasmoids play a major role in Saturn's global magnetospheric dynamics, especially at low p_{sw}. In other words, our model predicts major recurrent Kronian plasmoid events in otherwise quiet periods when nothing notable happens in the upstream solar wind, for example in the middle of a rarefaction region between two corotating interaction regions.

[37] **Acknowledgments.** This work was supported through the NASA Cassini Data Analysis Program NNX07AE54G.

[38] Masaki Fujimoto thanks the reviewers for their assistance in evaluating this article.

References

Achilleos, N., C. S. Arridge, C. Bertucci, C. M. Jackman, M. K. Dougherty, K. K. Khurana, and C. T. Russell (2008), Large-scale dynamics of Saturn's magnetopause: Observations by Cassini, *J. Geophys. Res.*, *113*, A11209, doi:10.1029/2008JA013265.

Arridge, C. S., C. T. Russell, K. K. Khurana, N. Achilleos, N. André, A. M. Rymer, M. K. Dougherty, and A. J. Coates (2007), Mass of Saturn's magnetodisc: Cassini observations, *Geophys. Res. Lett.*, *34*, L09108, doi:10.1029/2006GL028921.

Arridge, C. S., K. K. Khurana, C. T. Russell, D. J. Southwood, N. Achilleos, M. K. Dougherty, A. J. Coates, and H. K. Leinweber (2008), Warping of Saturn's magnetospheric and magnetotail current sheets, *J. Geophys. Res.*, *113*, A08217, doi:10.1029/2007JA012963.

Bagenal, F. (1994), Empirical model of the Io plasma torus: Voyager measurements, *J. Geophys. Res.*, *99*, 11,043–11,062, doi:10.1029/93JA02908.

Bagenal, F. (1997), Ionization source near Io from Galileo wake data, *Geophys. Res. Lett.*, *24*, 2111–2114, doi:10.1029/97GL02052.

Bagenal, F. (2007), The magnetosphere of Jupiter: Coupling the equator to the poles, *J. Atmos. Sol. Terr. Phys.*, *69*, 387–402, doi:10.1016/j.jastp.2006.08.012.

Broadfoot, A. L., et al. (1979), Extreme ultraviolet observations from Voyager 1 encounter with Jupiter, *Science*, *204*, 979–982.

Brown, M. E. (1994), Observation of mass loading in the Io plasma torus, *Geophys. Res. Lett.*, *21*, 847–850, doi:10.1029/94GL00564.

Burger, M. H., E. C. Sittler, R. E. Johnson, H. T. Smith, O. J. Tucker, and V. I. Shematovich (2007), Understanding the escape of water from Enceladus, *J. Geophys. Res.*, *112*, A06219, doi:10.1029/2006JA012086.

Cowee, M. M., N. Omidi, C. T. Russell, X. Blanco-Cano, and R. L. Tokar (2009), Determining ion production rates near Saturn's extended neutral cloud from ion cyclotron wave amplitudes, *J. Geophys. Res.*, *114*, A04219, doi:10.1029/2008JA013664.

Dougherty, M. K., K. K. Khurana, F. M. Neubauer, C. T. Russell, J. Saur, J. S. Leisner, and M. E. Burton (2006), Identification of a dynamic atmosphere at Enceladus with the Cassini magnetometer, *Science*, *311*, 1406–1409, doi:10.1126/science.1120985.

Hansen, K. C., T. I. Gombosi, D. L. De Zeeuw, C. P. T. Groth, and K. G. Powell (2000), A 3D global MHD simulation of Saturn's magnetosphere, *Adv. Space Res.*, *26*, 1681–1690, doi:10.1016/S0273-1177(00)00078-8.

Hansen, K. C., A. J. Ridley, G. B. Hospodarsky, N. Achilleos, M. K. Dougherty, T. I. Gombosi, and G. Tóth (2005), Global MHD simulations of Saturn's magnetosphere at the time of Cassini approach, *Geophys. Res. Lett.*, *32*, L20S06, doi:10.1029/2005GL022835.

Hill, T. W., et al. (2008), Plasmoids in Saturn's magnetotail, *J. Geophys. Res.*, *113*, A01214, doi:10.1029/2007JA012626.

Ip, W.-H. (1992), The nitrogen tori of Titan and Triton, *Adv. Space Res.*, *12*, 73–79, doi:10.1016/0273-1177(92)90379-C.

Jackman, C. M., C. T. Russell, D. J. Southwood, C. S. Arridge, N. Achilleos, and M. K. Dougherty (2007), Strong rapid dipolarizations in Saturn's magnetotail: In situ evidence of reconnection, *Geophys. Res. Lett.*, *34*, L11203, doi:10.1029/2007GL029764.

Jackman, C. M., et al. (2008), A multi-instrument view of tail reconnection at Saturn, *J. Geophys. Res.*, *113*, A11213, doi:10.1029/2008JA013592.

Joy, S. P., M. G. Kivelson, R. J. Walker, K. K. Khurana, C. T. Russell, and T. Ogino (2002), Probabilistic models of the Jovian magnetopause and bow shock locations, *J. Geophys. Res.*, *107*(A10), 1309, doi:10.1029/2001JA009146.

Jurac, S., M. A. McGrath, R. E. Johnson, J. D. Richardson, V. M. Vasyliūnas, and A. Eviatar (2002), Saturn: Search for a missing water source, *Geophys. Res. Lett.*, *29*(24), 2172, doi:10.1029/2002GL015855.

Khurana, K. K., M. K. Dougherty, C. T. Russell, and J. S. Leisner (2007), Mass loading of Saturn's magnetosphere near Enceladus, *J. Geophys. Res.*, *112*, A08203, doi:10.1029/2006JA012110.

Kivelson, M. G., and D. J. Southwood (2005), Dynamical consequences of two modes of centrifugal instability in Jupiter's outer magnetosphere, *J. Geophys. Res.*, *110*, A12209, doi:10.1029/2005JA011176.

Kivelson, M. G., K. K. Khurana, R. J. Walker, J. Warnecke, C. T. Russell, J. A. Linker, D. J. Southwood, and C. Polanskey (1996), Io's interaction with the plasma torus: Galileo magnetometer report, *Science*, *274*, 396–398.

Krupp, N. (2007), New surprises in the largest magnetosphere of our solar system, *Science*, *318*, 216–217, doi:10.1126/science.1150448.

Leisner, J. S., C. T. Russell, M. K. Dougherty, X. Blanco-Cano, R. J. Strangeway, and C. Bertucci (2006), Ion cyclotron waves in Saturn's E ring: Initial Cassini observations, *Geophys. Res. Lett.*, *33*, L11101, doi:10.1029/2005GL024875.

McComas, D. J., F. Allegrini, F. Bagenal, F. Crary, R. W. Ebert, H. Elliott, A. Stern, and P. Valek (2007), Diverse plasma populations and structures in Jupiter's magnetotail, *Science*, *318*, 217–220, doi:10.1126/science.1147393.

Pontius, D. H., Jr., and T. W. Hill (1982), Departure from corotation of the Io plasma torus: Local plasma production, *Geophys. Res. Lett.*, *9*, 1321–1324, doi:10.1029/GL009i012p01321.

Pontius, D. H., Jr., and T. W. Hill (2006), Enceladus: A significant plasma source for Saturn's magnetosphere, *J. Geophys. Res.*, *111*, A09214, doi:10.1029/2006JA011674.

Porco, C. C., et al. (2006), Cassini observes the active South Pole of Enceladus, *Science*, *311*, 1393–1401, doi:10.1126/science.1123013.

Powell, K. G., P. L. Roe, T. J. Linde, T. I. Gombosi, and D. L. De Zeeuw (1999), A solution-adaptive upwind scheme for ideal magnetohydrodynamics, *J. Comput. Phys.*, *154*, 284–309.

Richardson, J. D. (1998), Thermal plasma and neutral gas in Saturn's magnetosphere, *Rev. Geophys.*, *36*, 501–524, doi:10.1029/98RG01691.

Richardson, J. D., and S. Jurac (2004), A self-consistent model of plasma and neutrals at Saturn: The ion tori, *Geophys. Res. Lett.*, *31*, L24803, doi:10.1029/2004GL020959.

Richardson, J. D., A. Eviatar, M. A. McGrath, and V. M. Vasyliūnas (1998), OH in Saturn's magnetosphere: Observations and implications, *J. Geophys. Res.*, *103*, 20,245–20,256, doi:10.1029/98JE01127.

Ridley, A. J., T. I. Gombosi, and D. L. De Zeeuw (2004), Ionospheric control of the magnetosphere: Conductance, *Ann. Geophys.*, *22*, 567–584.

Russell, C. T., K. K. Khurana, M. G. Kivelson, and D. E. Huddleston (2000), Substorms at Jupiter: Galileo observations of transient reconnection in the near tail, *Adv. Space Res.*, *26*, 1499–1504, doi:10.1016/S0273-1177(00)00084-3.

Russell, C. T., Y. L. Wang, X. Blanco-Cano, and R. J. Strangeway (2001), The Io mass-loading disk: Constraints provided by ion cyclotron wave observations, *J. Geophys. Res.*, *106*, 26,233–26,242, doi:10.1029/2001JA900029.

Saur, J., D. F. Strobel, F. M. Neubauer, and M. E. Summers (2003), The ion mass loading rate at Io, *Icarus*, *163*, 456–468, doi:10.1016/S0019-1035(03)00085-X.

Sheeley, N. R., D. D.-H. Lee, K. P. Casto, Y.-M. Wang, and N. B. Rich (2009), The structure of streamer blobs, *Astrophys. J.*, *694*, 1471–1480, doi:10.1088/0004-637X/694/2/1471.

Sheeley, N. R., Jr., and Y.-M. Wang (2007), In/out pairs and the detachment of coronal streamers, *Astrophys. J.*, *655*, 1142–1156, doi:10.1086/510323.

Shemansky, D. E. (1980), Mass-loading and diffusion-loss rates of the Io plasma torus, *Astrophys. J.*, *242*, 1266–1277, doi:10.1086/158557.

Shemansky, D. E., P. Matheson, D. T. Hall, H.-Y. Hu, and T. M. Tripp (1993), Detection of the hydroxyl radical in the Saturn magnetosphere, *Nature*, *363*, 329–331, doi:10.1038/363329a0.

Tokar, R. L., et al. (2008), Cassini detection of water-group pick-up ions in the Enceladus torus, *Geophys. Res. Lett.*, *35*, L14202, doi:10.1029/2008GL034749.

Tóth, G., et al. (2005), Space Weather Modeling Framework: A new tool for the space science community, *J. Geophys. Res.*, *110*, A12226, doi:10.1029/2005JA011126.

Vasyliūnas, V. M. (1983), *Plasma Distribution and Flow*, pp. 395–453, Cambridge Univ. Press, New York.

Vasyliūnas, V. M. (2008), Comparing Jupiter and Saturn: Dimensionless input rates from plasma sources within the magnetosphere, *Ann. Geophys.*, *26*, 1341–1343.

Wang, Y., C. T. Russell, and J. Raeder (2001), The Io mass-loading disk: Model calculations, *J. Geophys. Res.*, *106*, 26,243–26,260, doi:10.1029/2001JA900062.

Wang, Y.-M., and N. R. Sheeley Jr. (2006), Observations of flux rope formation in the outer corona, *Astrophys. J.*, *650*, 1172–1183, doi:10.1086/506611.

Wang, Y.-M., N. R. Sheeley, D. G. Socker, R. A. Howard, and N. B. Rich (2000), The dynamical nature of coronal streamers, *J. Geophys. Res.*, *105*, 25,133–25,142, doi:10.1029/2000JA000149.

Woch, J., N. Krupp, and A. Lagg (2002), Particle bursts in the Jovian magnetosphere: Evidence for a near-Jupiter neutral line, *Geophys. Res. Lett.*, *29*(7), 1138, doi:10.1029/2001GL014080.

Zieger, B., and K. C. Hansen (2008), Statistical validation of a solar wind propagation model from 1 to 10 AU, *J. Geophys. Res.*, *113*, A08107, doi:10.1029/2008JA013046.

D. L. De Zeeuw, T. I. Gombosi, and K. C. Hansen, Department of Atmospheric, Oceanic and Space Sciences, University of Michigan, 2455 Hayward St., Ann Arbor, MI 48109, USA. (kenhan@umich.edu)

B. Zieger, Space Research Institute, Austrian Academy of Sciences, Schmiedlstrasse 6, 8042 Graz, Austria. (bertalan.zieger@oeaw.ac.at)